High-Resolution Crystal Structure of Plant Carboxylesterase AeCXE1, from *Actinidia eriantha*, and Its Complex with a High-Affinity Inhibitor Paraoxon[†,‡]

Nadeesha R. Ileperuma,[§,||] Sean D. G. Marshall,[§,||,⊥] Christopher J. Squire,[§] Heather M. Baker,[§] John G. Oakeshott,[@] Robyn J. Russell,[@] Kim M. Plummer,[§,#] Richard D. Newcomb,[||] and Edward N. Baker*[,§]

School of Biological Sciences, University of Auckland, Auckland, New Zealand, Horticulture and Food Research Institute of New Zealand Limited (HortResearch), Mount Albert Research Centre, Auckland, New Zealand, and Entomology Division, Commonwealth Scientific and Industrial Research Organization (CSIRO), Canberra, Australia

Received October 1, 2006; Revised Manuscript Received December 11, 2006

ABSTRACT: Carboxylesterases (CXEs) are widely distributed in plants, where they have been implicated in roles that include plant defense, plant development, and secondary metabolism. We have cloned, overexpressed, purified, and crystallized a carboxylesterase from the kiwifruit species *Actinidia eriantha* (AeCXE1). The structure of AeCXE1 was determined by X-ray crystallography at 1.4 Å resolution. The crystal structure revealed that AeCXE1 is a member of the α/β-hydrolase fold superfamily, most closely related structurally to the hormone-sensitive lipase subgroup. The active site of the enzyme, located in an 11 Å deep hydrophobic gorge, contains the conserved catalytic triad residues Ser169, Asp276, and His306. Kinetic analysis using artificial ester substrates showed that the enzyme can hydrolyze a range of carboxylester substrates with acyl groups ranging from C2 to C16, with a preference for butyryl moieties. This preference was supported by the discovery of a three-carbon acyl adduct bound to the active site Ser169 in the native structure. AeCXE1 was also found to be inhibited by organophosphates, with paraoxon (IC_{50} = 1.1 μM) a more potent inhibitor than dimethylchlorophosphate (DMCP; IC_{50} = 9.2 μM). The structure of AeCXE1 with paraoxon bound was determined at 2.3 Å resolution and revealed that the inhibitor binds covalently to the catalytic serine residue, with virtually no change in the structure of the enzyme. The structural information for AeCXE1 provides a basis for addressing the wider functional roles of carboxylesterases in plants.

Carboxylesterases (EC 3.1.1.1) are found in all kingdoms of life. These enzymes catalyze the hydrolysis of carboxylic esters into their corresponding alcohols and carboxylic acids. A large number of carboxylesterases from animals and microbes have been cloned, characterized, and shown to be involved in a broad range of functions, including the processing or degradation of neurotransmitters (*1*), hormones (*2*), and xenobiotics (*3*−*5*). Substrate specificities vary widely, with some enzymes displaying highly specific activity toward particular substrates [e.g., acetylcholinesterase (*6*)], whereas others have activity against a broad range of substrates (*7*).

Although carboxylesterases are thought to participate in a broad range of plant processes, the plant carboxylesterases are less well characterized than their animal and microbial counterparts, and in most cases, physiological roles have not yet been assigned. Multiple carboxylesterase isoenzymes are expressed in many plant tissues, including fruit, leaves, and roots (*8*−*10*). Biochemical studies have shown that these enzymes can hydrolyze a wide range of esters that are potentially involved in processes such as plant development, detoxification, plant defense, and secondary metabolism (*11*−*14*). Interestingly, some plant carboxylesterases have evolved new activities. In legumes, at least two carboxylesterases have attained additional dehydratase activity and are involved in isoflavone biosynthesis (*15*). In rice, a putative carboxylesterase has lost carboxylesterase activity and functions as a receptor for gibberellic acid (*16*).

A family of 20 plant carboxylesterases has recently been identified from the *Arabidopsis thaliana* genome (AtCXE1−20) and their tissue expression examined, showing that most are expressed throughout the plant (*12*). Multiple-sequence alignment identified sequence motifs consistent with these putative carboxylesterases being members of the α/β-hydrolase fold superfamily (*17*−*19*), to which all animal and microbial carboxylesterases of known three-dimensional structure belong. Members of this superfamily share a characteristic α/β fold, which supports an essential nucleophile (Nuc), usually serine, in a catalytic Nuc-His-Asp/Glu triad. The nucleophile is located within a conserved Gly-X-Nuc-X-Gly motif in a sharp turn (the nucleophilic elbow) between β-strand 5 and α-helix 3. This allows the efficient

[†] This work was supported by funding from the New Economy Research Fund of New Zealand. S.D.G.M. was the recipient of a Bright Futures Enterprise Scholarship from the Foundation for Research, Science and Technology (New Zealand).

[‡] Atomic coordinates have been deposited in the Protein Data Bank as entries 2o7r (native AeCXE1) and 2o7v (paraoxon complex of AeCXE1).

* To whom correspondence should be addressed. Phone: +64-9-373-7599. Fax: +64-9-373-7414. E-mail: ted.baker@auckland.ac.nz.

[§] University of Auckland.

[||] Mount Albert Research Centre.

[⊥] Current address: AgResearch, Canterbury Agriculture & Science Centre, Lincoln, New Zealand.

[@] Commonwealth Scientific and Industrial Research Organization.

[#] Current address: Botany Department, La Trobe University, Melbourne, Victoria 3086, Australia.

10.1021/bi062046w CCC: $37.00
Published on Web 01/26/2007

presentation of the nucleophile to the substrate and positions the enzyme−substrate intermediate within hydrogen bonding distance of an "oxyanion hole", leading to the stabilization of the transition state (*20*).

No three-dimensional structural information for any plant carboxylesterase is yet available. In view of their wide distribution in plants and their likely importance in functions such as plant development, defense against pathogens, and secondary metabolism (*11*, *13*, *14*), we have expressed, characterized, and crystallized the putative carboxylesterase, AeCXE1,[1] from kiwifruit (*Actinidia eriantha*). Here we report the three-dimensional structure of AeCXE1 at 1.4 Å resolution, characterize its ability to hydrolyze a range of esters, and describe its complex with the organophosphate inhibitor paraoxon at 2.3 Å resolution.

MATERIALS AND METHODS

Cloning and Expression. The *AeCXE1* gene was identified from a kiwifruit (*A. eriantha* Benth.) EST database (unpublished data). The entire AeCXE1 coding region was PCR-amplified and subcloned into the *Bam*HI−*Hin*dIII sites of the pQE30 expression vector (Qiagen, Valencia, CA) to produce the overexpression construct His_6-AeCXE1. The plasmid containing His_6-AeCXE1 was transformed into *Escherichia coli* M15 cells for overexpression using the QIAexpress system (Qiagen). Recombinant *E. coli* M15 cells were grown at 37 °C to an OD_{600} of 0.6−0.8, cooled to 20 °C on ice, induced with 1 mM isopropyl β-D-1-thiogalactopyranoside, grown for a further 18 h at 20 °C, and harvested by centrifugation. Cell pellets were resuspended in lysis buffer comprising 5 mM imidazole, 0.5 mM NaCl, 20 mM TAPS (pH 9.0), and 10% glycerol. The use of TAPS as a buffer was essential to prevent aggregation, and samples prepared for crystallographic studies additionally contained EDTA-free protease inhibitor cocktail tablets (Roche) as a precaution against any possible proteolysis that might lead to heterogeneity. The cells were disrupted using an Emulsiflex-CS high-pressure homogenizer (Avestin Inc.), and the resulting cell debris was removed by centrifugation at 15700*g*.

Protein Purification and Crystallization. N-Terminally His_6-tagged recombinant AeCXE1 was purified from the supernatant by Ni^{2+} affinity chromatography using a 5 mL HiTrap chelating HP column (Amersham Biosciences). Bound protein was eluted from the column using a linear imidazole gradient from 0.005 to 1 M. Fractions containing the recombinant AeCXE1 enzyme were identified by SDS−PAGE, pooled, and concentrated. The concentrated protein was further purified by size exclusion chromatography using a Superdex 200 column (Amersham Biosciences) and eluted in 50 mM TAPS (pH 9.0) and 150 mM NaCl. Fractions containing recombinant AeCXE1 were pooled and concentrated to 9.8 mg/mL. Analysis by dynamic light scattering (DynaPro 200, Protein Solutions) prior to crystal trials gave a C_p/R_h value of 26%, indicating moderate monodispersity.

Crystallization conditions were identified using a Cartesian HONEYBEE nanoliter dispensing robot (Genomic solutions) with a 480-condition crystallization screen (*21*). Crystals were grown at room temperature in sitting drops by mixing 100 nL of the protein solution (9.8 mg/mL) with an equal volume of reservoir solution. The best crystallization condition for AeCXE1 was 21% mPEG 5000 with 0.2 M malic/KOH (pH 5.5). Rod-shaped crystals formed within 2−3 days and grew larger over a 2 week period with the longest crystal growing to 0.4 mm. The crystals were monoclinic, in space group *C*2, with one molecule per asymmetric unit and the following unit cell dimensions: $a = 156.27$ Å, $b = 53.78$ Å, $c = 42.29$ Å, and $\beta = 102.55°$.

A mercury derivative was produced by soaking a crystal in a 10 μL drop of reservoir solution supplemented with 0.25 mM ethylmercuric chloride at room temperature. The crystal was then back-soaked in a 10 μL drop of reservoir solution to remove excess heavy metal reagent. A crystal of AeCXE1 in complex with its inhibitor paraoxon was obtained by soaking the crystal in a 1 μL drop of reservoir solution supplemented with 0.185 mM paraoxon for 1 h at room temperature.

Data Collection. Prior to data collection, crystals were briefly soaked in a cryoprotectant solution comprising 80% (v/v) reservoir solution and 20% (v/v) glycerol and immediately flash-frozen in liquid nitrogen. X-ray diffraction data for the native and mercury derivative crystals were collected at 100 K on beamlines 9-1 and 1-5, respectively, at the Stanford Synchrotron Radiation Laboratory (Menlo Park, CA), using ADSC Q 315 detectors. A native data set to 1.45 Å was collected from the native crystal, while multiwavelength anomalous diffraction data to 2.6 Å resolution were collected at three wavelengths (peak, inflection, and remote) around the mercury edge from the mercury derivative crystal. Data for the AeCXE1−paraoxon complex crystal were collected at 110 K using a Rigaku RU-H3R rotating anode X-ray generator equipped with osmic mirrors and a MAR 345 image plate detector. Diffraction data were collected to 2.3 Å resolution with Cu Kα radiation ($\lambda = 1.5418$ Å).

All data for the native and mercury derivative crystals were processed using the Denzo/HKL package (*22*), while the data for the AeCXE1−paraoxon complex crystal were processed using MOSFLM (*23*). Details of the data collection and processing statistics are given in Table 1.

Structure Determination and Refinement. The three-dimensional structure of AeCXE1 was determined by multiwavelength anomalous dispersion (MAD), using the three-wavelength diffraction data from the mercury derivative crystal. Three mercury sites were identified, all attached to accessible cysteine residues (Cys109, Cys243, and Cys273), and were refined using SOLVE (*24*), giving a figure of merit of 0.48. The SOLVE map was subsequently input to RESOLVE (*25*, *26*) for density modification. Autobuilt models from RESOLVE and ARP/wARP (*27*) were combined to give a starting model for manual building in COOT (*28*). The partial model was used for molecular replacement into the native structure using MOLREP and the new model submitted to ARP/wARP (*27*) for autotracing and rebuilding, giving 287 residues from the total of 338. This model was refined with REFMAC (*29*), and a further 18 residues were added manually from $2F_o - F_c$ maps (including experimental

[1] Abbreviations: CXE, carboxylesterase; AeCXE1, carboxylesterase 1 from *Actinidia eriantha*; DMCP, dimethyl chlorophosphate; EST, expressed sequence tag; mPEG, methoxypolyethylene glycol; TAPS, *N*-tris(hydroxymethyl)methyl-3-aminopropanesulfonic acid; 4MU, 4-methylumbelliferyl; rms, root-mean-square; HSL, hormone-sensitive lipase.

Table 1: Data Collection and Processing Statistics

	native	Hg peak	Hg inflection	Hg remote	AeCXE1−paraoxon complex
wavelength (Å)	0.97907	1.00611	1.00888	0.95362	1.5418
space group	*C*2	*C*2			*C*2
cell parameters					
a (Å)	156.26	154.75			156.08
b (Å)	53.78	53.82			53.91
c (Å)	42.29	42.35			42.36
β (deg)	102.5	102.5			102.2
resolution range (outer shell) (Å)	50.0−1.4 (1.45−1.40)	50.0−2.5 (2.59−2.5)	50.0−2.5 (2.59−2.5)	50.0−2.5 (2.59−2.5)	33.5−2.3 (2.42−2.30)
total no. of observations	141110	37511	37742	40886	66554
no. of unique reflections	63217	10565	10593	11333	14481
completeness (%)	93.2 (61.8)	88.4 (49.4)	87.5 (48.1)	94.6 (67.0)	94.1 (89.7)
I/σ	22.6 (1.8)	24.6 (4.03)	23.6 (3.5)	22.5 (3.8)	14.8 (3.7)
R_{sym} (%)	4.2 (43.8)	9.1 (34.5)	8.9 (37.7)	9.5 (36.5)	9.7 (42.6)
MAD phasing					
no. of Hg sites		3			
overall figure of merit					
Solve		0.48			
Resolve		0.62			

Table 2: Refinement Statistics

	native	paraoxon complex
resolution range (Å)	50.0−1.4	33.5−2.3
no. of reflections (working/test)	57862/3305	13035/723
R_{cryst}/R_{free}	0.199/0.218	0.187/0.248
no. of atoms (non-hydrogen)		
protein atoms	2403	2403
water molecules	217	58
ligands	7	8
average *B* factor (Å^2)		
protein	16.4	27.5
water	26.3	26.2
ligand	27.2	25.9
rms deviations from standard values		
bond lengths (Å)	0.021	0.020
bond angles (deg)	1.92	1.88
residues in the most favored region of the Ramachandran plot (%)	90.5	87.5

phases). Water molecules added during ARP/wARP were only retained on the basis of the potential to form hydrogen bonds with the neighboring residues and at locations where $F_o - F_c$ density exceeded 3σ. Nonprotein density was observed covalently linked to Ser169 and was modeled as a transition state intermediate, using SYBYL 7.0 (Tripos Associates Inc.) and manually docked into position. This intermediate was then included in further rounds of refinement.

The structure of the AeCXE1−paraoxon complex was determined by molecular replacement using the native structure and refined with REFMAC. All maps displayed clear density for paraoxon, allowing it to be modeled with SYBYL 7.0 and manually docked into position. Details of the structure refinement are given in Table 2.

Both final models (native and paraoxon-complexed crystals) consisted of 305 residues, with only N-terminal residues 1−17, the loop of residues 250−254, and C-terminal residues 329−338 having no interpretable density. The final native AeCXE1 model contains 140 water molecules and a putative transition state intermediate molecule, whereas the final AeCXE1−paraoxon complex contains 75 water molecules and a paraoxon molecule. The protein geometries of both models were monitored during the course of refinement using PROCHECK (*30*), with the native and paraoxon complex models having 90.5 and 87.5% of their residues in the most favored regions of the Ramachandran plot, respectively. In both models, Ser169 is located in the disallowed region of the Ramachandran plot.

Kinetic and Inhibition Studies. Activity assays were carried out with enzyme samples prepared without the presence of protease inhibitor tablets and should represent the fully active enzyme. The esterase activity of AeCXE1 was determined fluorimetrically by measuring the hydrolysis rates of various 4-methylumbelliferyl (4MU) esters. Hydrolysis was assessed at 25 °C using a POLARstar fluorimeter, with filters set at 355 and 445 nm (excitation and emission, respectively). Reactions were initiated by the addition of 50 μL of a substrate solution to 50 μL of an enzyme solution, in 25 mM Tris-HCl (pH 8.0) with changes in fluorescence recorded over 10 min. Care was taken to use substrate concentrations below the maximum solubility of each ester, and preliminary K_m estimation experiments were conducted to determine a concentration range for each substrate that would bracket the final estimated K_m values. Estimated rates were the average of three replicate reactions and were corrected for substrate autohydrolysis. Measurements were taken for 4MU acetate (Sigma), 4MU butyrate (Sigma), 4MU heptanoate (Sigma), 4MU octanoate (Sigma), 4MU laurate (Research Organics, Cleveland, OH), and 4MU palmitate (Sigma). A minimum of eight substrate concentrations were used to estimate K_m values using nonlinear regression analysis of initial rate data with the program Origin 7.5 SR4 (OriginLab, 2004). Values of k_{cat} were calculated from the V_{max} using an estimate of the molar amount of active sites, following the method of Devonshire et al. (*49*).

Inhibition by the organophosphates dimethylchlorophosphate (DMCP; Sigma) and diethyl *p*-nitrophenyl phosphate (paraoxon; Supelco, Bellefonte, PA) was tested by measuring the residual hydrolytic activity of AeCXE1 toward 4MU butyrate (final concentration of 10 μM) after preincubation of enzyme with inhibitor for 10 min. Concentrations that were used were 0.001−1000 μM and were used to calculate the IC_{50} value (50% inhibitory concentration) for each inhibitor using the Origin version 7.5 graphing and data

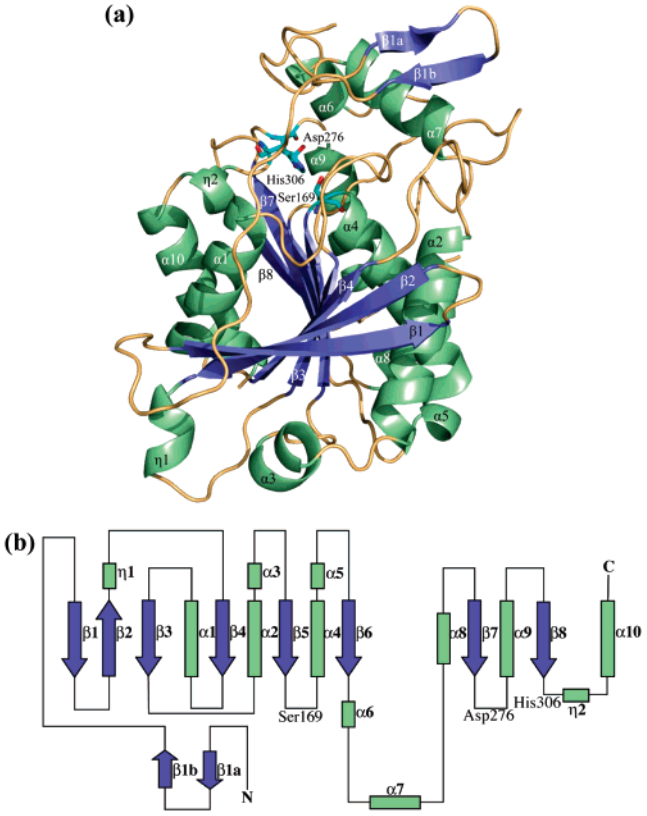

FIGURE 1: (a) Overall fold of AeCXE1, with β-strands colored blue and α-helices green. The residues of the catalytic triad are shown as sticks. The figure was generated using Pymol (*48*). (b) Topology diagram for AeCXE1. The color scheme corresponds to the colors used for β-strands and α-helices in panel a.

analysis software package (OriginLab Corp., Northampton, MA).

RESULTS

Overall Structure. *A. eriantha* carboxylesterase AeCXE1 is a monomeric, single-domain protein with approximate dimensions of 51 Å × 46 Å × 38 Å. The molecule (338 amino acid residues, 36 kDa) has the characteristic α/β-hydrolase fold (*17*). The central eight-stranded β-sheet (β1−β8) has helices packed on both faces, with helices α1 and α10, plus a short 3_{10}-helix η2, on one side, and helices α2, α4, α5, α8, and α9 on the other (Figure 1). The central β-sheet has a left-handed superhelical twist, with the first and last strands oriented at an angle of approximately 90°. A small β-sheet comprising two antiparallel β-strands (β1a and β1b) is located near the N-terminus, connected to the central β-sheet by an extended loop. When compared with the generalized α/β-hydrolase fold described by Ollis et al. (*17*), the AeCXE1 structure contains seven additional helical insertions in the central β-sheet, α3, α5−α8, η1, and η2 (Figure 1). Insertions into the central core are common in proteins with the α/β-hydrolase fold and are thought to regulate the substrate specificities of these enzymes (*18*, *19*). Of the insertions in the AeCXE1 structure, three helices, α6, α7, and η2, are located close to the active site of the enzyme and may help determine the substrate specificity of the enzyme.

A search of the Protein Data Bank for structural homologues of AeCXE1, using SSM [http://www.ebi.ac.uk/msd-srv/ssm (*31*)], identified the closest homologues as AFEST, a hyperthermophilic carboxylesterase from *Arachaeglobus fulgidus* (PDB entry 1JJI) (*32*), the thermophilic carboxylesterase EST2 from *Alicyclobacillus acidocaldarius* (PDB entry 1EVQ) (*33*), the thermophilic and thermostable carboxylesterase ESTE1 from a metagenomic library (PDB entry 2C7B) (Byun et al., unpublished), and the brefeldin A esterase (BAEST) from *Bacillus subtilis* (PDB entry 1JKM) (*34*). Overall, AFEST had the highest *Z* score of 10.9 and a root-mean-square difference (rmsd) of 1.81 Å over the Cα positions of 242 aligned residues, but BAEST, with a slightly lower *Z* score, was the best match on Cα positions, with an rmsd of 1.77 Å over 241 aligned residues.

The four enzymes listed above are 24−25% identical in sequence with AeCXE1, with 27 residues being completely conserved among all five enzymes (Figure 2). The majority of the conserved residues are found near the C-terminal ends of the β-strands, in the active site region, and include the residues of the catalytic triad and two of the three oxyanion hole residues, which are Gly92, Gly93, and Ala170 in AeCXE1. The third oxyanion hole residue is Gly201 in BAEST, but Ala in the other four enzymes. AFEST, EST2, and BAEST all belong to the hormone-sensitive lipase subfamily in which a hydrophobic lid domain covers the active site. This lid structure is usually contributed by two separate helical regions, one comprising the N-terminal residues and the other comprising insertions to the central β-sheet between β6 and β7. Although AeCXE1 also contains a two-strand β-sheet at the N-terminus and similar helical insertions at the corresponding positions in the central β-sheet (between β6 and β7 in AeCXE1), it lacks the pronounced lid seen in the three structures mentioned above.

Active Site. The active site of AeCXE1 was identified by the location of the nucleophilic serine, Ser169, within the conserved pentapeptide sequence Gly-X-Ser-X-Gly. The catalytic triad comprises Ser169, His306, and Asp276, and an oxyanion hole is formed by the peptide NH groups of Gly92, Gly93, and Ala170 (Figure 3). Ser169 is located in the characteristic "nucleophilic elbow" position, a sharp turn at the apex of the β5−α4 loop, placing it in a normally unfavorable region of the Ramachandran plot. Its Φ and Ψ angles (60° and −124°, respectively) are, however, characteristic of other α/β-hydrolases (*17*−*20*). Ser169 Oγ is within hydrogen bonding distance of Nϵ2 of His306 (2.74 Å), which is in turn hydrogen bonded through Nδ1 to Oδ1 of Asp276 (2.79 Å). The three catalytic triad residues, Ser169, Asp276, and His306, are located on the β5−α4, β7−α10, and β8−α11 loops, respectively, placing them on the C-terminal side of the β-sheet.

The catalytic triad and oxyanion hole are located in a deep gorge that is characteristic of many α/β-hydrolase fold proteins. In AeCXE1, this catalytic gorge is funnel-shaped with a wide opening (∼13 Å) which narrows toward the bottom, extending ∼11 Å into the enzyme. The catalytic triad and oxyanion hole residues are located about two-thirds of the way into the gorge, with their side chains protruding into it. The gorge is lined with mainly hydrophobic residues, from the loops following β3−β8, α6, and α7, and is terminated with a small pocket below the catalytic residues, with Trp231 at the bottom. Near the opening is a deeply hydrophobic patch contributed by the N-terminal residues Leu18−Ile24. A continuous stretch of hydrophobicity extends from the

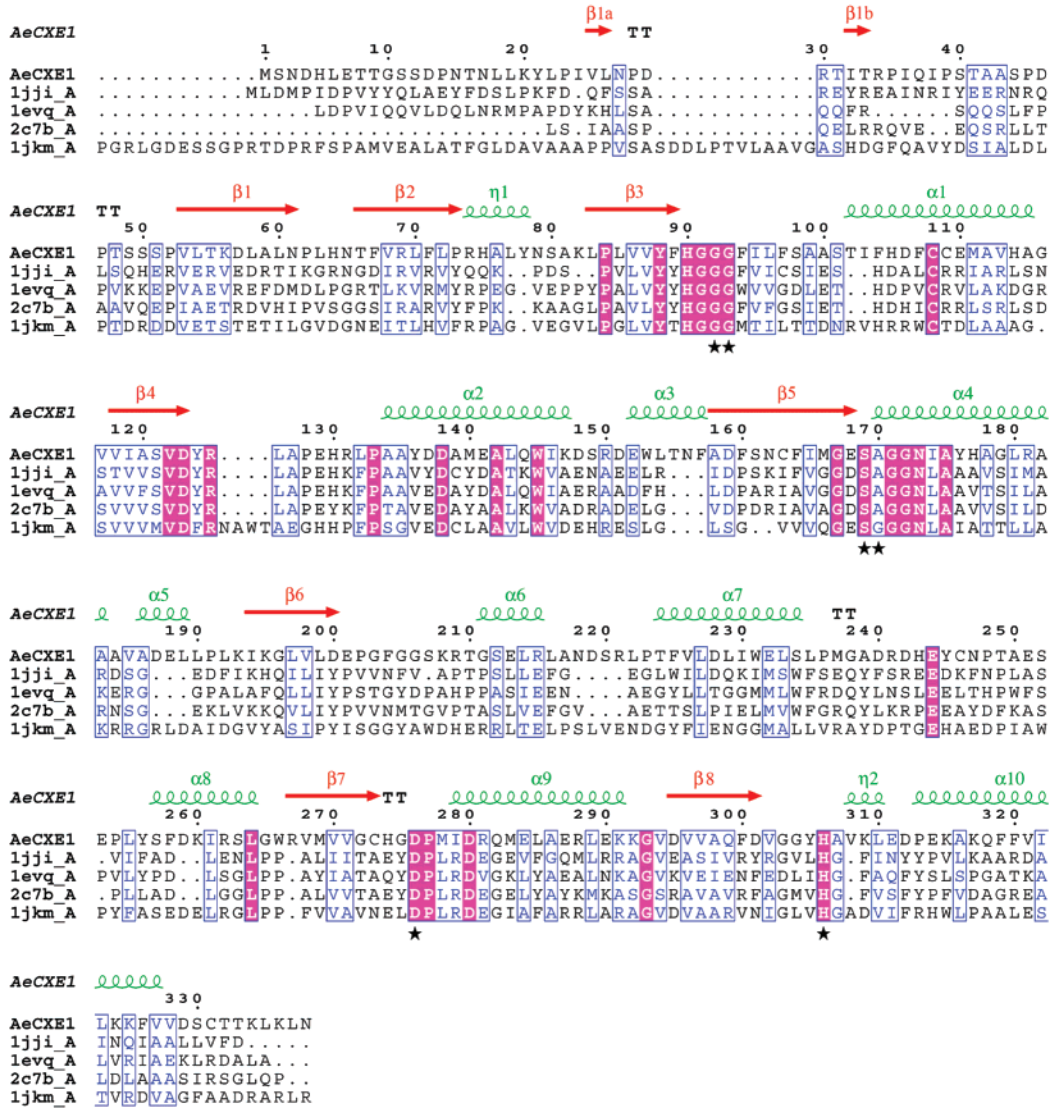

FIGURE 2: Structure-based sequence alignment of AeCXE1 with the four closest structural homologues identified by the program SSM, hyperthermophilic carboxylesterase from *Archaeglobus fulgidus* (1JJI), the thermophilic carboxylesterase EST2 from *Alicyclobacillus acidocaldarius* (1EVQ), thermophilic and thermostable carboxylesterase ESTE1 from a metagenomic library (2C7B), and brefeldin A esterase from *B. subtilis* (1JKMA). Residues that are fully conserved (pink background) and conservatively substituted (blue) within the five sequences are denoted. The catalytic triad residues and oxyanion hole residues are denoted with stars below the alignment. The secondary structure elements and the residue numbering for AeCXE1 are displayed above the sequence.

bottom of the gorge toward the opening with a number of well-defined hydrophobic pockets, which could act as putative alcohol binding pockets. This hydrophobic stretch is mainly contributed by the residues of the loop following β-strand 3.

Unexpectedly, nonprotein electron density, which persisted in all $2F_o - F_c$ maps during refinement of the native structure, was found adjacent to the nucleophile Ser169. This density merged with the density for the Ser169 Oγ atom, implying a covalent linkage. The shape of the density was consistent with a covalently bound acyl group, with continuous density extending into the hydrophobic pocket beneath the catalytic site and strong density reaching into the oxyanion hole (Figure 3). Similar acyl adducts have been found in other α/β-hydrolases, for example, the thermophilic carboxylesterase EST2 (*33*). In this case, the shape of the density rules out species from the crystallization solution, such as a TAPS-derived sulfonyl moiety. We assume that it is most likely derived from a serine protease inhibitor present in the Roche protease inhibitor cocktail tablets that were added during purification of AeCXE1 for crystallization, although we cannot exclude the possibility that some cellular metabolite from the *E. coli* host cells may have bound. An acyl intermediate with a three-carbon chain, covalently attached to Ser169 Oγ, was therefore modeled into the density and refined. The hydrocarbon chain is directed toward Trp231 at the bottom of the catalytic gorge and thus identifies the acyl binding pocket of the enzyme (Figure 3a). The acyl oxygen points toward the oxyanion hole of AeCXE1, in position to accept hydrogen bonds from the peptide NH groups of residues Gly92, Gly93, and Ala170 (Figure 3b).

Substrate Specificity and Kinetics. Kinetic parameters for the hydrolysis of 4MU esters with varying acyl chain length are given in Table 3. The K_m values decrease markedly with an increase in chain length, from 33 μM for acetyl to 24 nM for the 16-carbon palmityl ester, implying a high affinity for the longer chain esters. Catalytic activity (k_{cat}) also decreases markedly with an increase in chain length, however, with only low levels of activity against the long chain lauryl and palmityl esters. The optimum substrate

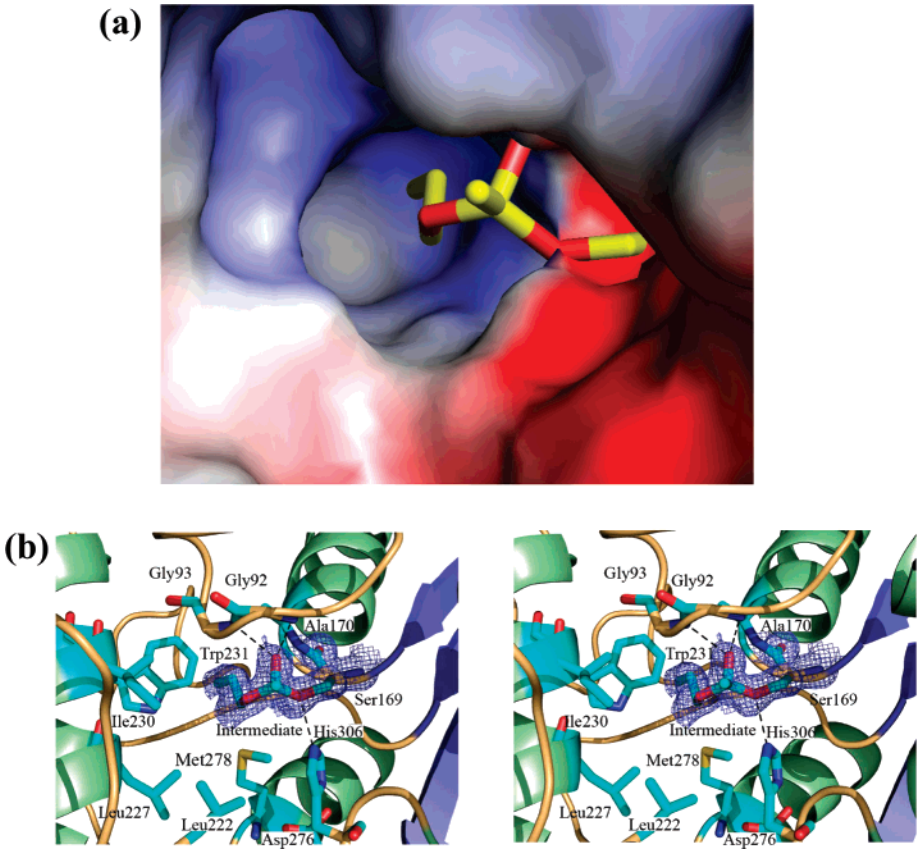

FIGURE 3: (a) Surface diagram of the AeCXE1 catalytic gorge with the intermediate shown in stick mode. (b) Stereoview of the AeCXE1 catalytic gorge with the bound intermediate shown built into its electron density from a bias-removed $2F_o - F_c$ omit map, contoured at 1.5σ. Key residues of the catalytic gorge are shown as sticks with the hydrogen bonds shown as dashed black lines. These images were generated using Pymol (*48*).

Table 3: Kinetic Parameters for 4MU Ester Hydrolysis by AeCXE1[a]

4MU ester[b]	K_m (μM)	k_{cat} (s^{-1})	k_{cat}/K_m ($\times 10^6$ s^{-1} M^{-1})
acetate (C_2)	33.3 ± 4.5	1.61 ± 0.10	0.0483 ± 0.0035
butyrate (C_4)	16.7 ± 2.1	10.1 ± 0.5	0.604 ± 0.048
heptanoate (C_7)	19.1 ± 4.7	2.00 ± 0.28	0.104 ± 0.012
octanoate (C_8)	6.34 ± 0.99	0.162 ± 0.011	0.0257 ± 0.0024
laurate (C_{12})	0.117 ± 0.023	0.010 ± 0.001	0.088 ± 0.012
palmitate (C_{16})	0.024 ± 0.005	0.0018 ± 0.0001	0.0732 ± 0.0130

[a] All experiments were conducted in 50 mM Tris-HCl (pH 8.0) at 25 °C. Standard errors represent the standard error of the mean calculated from a minimum of three experiments. [b] The number of carbon atoms in the acyl chain is shown in parentheses.

specificity, as measured by the specificity constant k_{cat}/K_m, is found for the 4MU butyrate ester.

Organophosphate Inhibition of AeCXE1. Inhibition assays demonstrate that both DMCP and paraoxon inhibit AeCXE1 with high affinity but that paraoxon is an order of magnitude more potent (Figure 4). The estimated IC_{50} values are 9.2 and 1.1 μM for DMCP and paraoxon, respectively. Electron density maps for the paraoxon-soaked crystals displayed clear density for a covalently bound diethyl phosphate moiety (Figure 5). The density also revealed that the *p*-nitrophenyl leaving group of paraoxon had been cleaved off during crystal soaking, thereby leaving a tetrahedral product reminiscent of the first transition state formed during carboxyl ester hydrolysis. The phosphate group of paraoxon is clearly defined by tetrahedral density and is covalently bound to Ser169 Oγ, with the O1 atom of paraoxon placed ap-

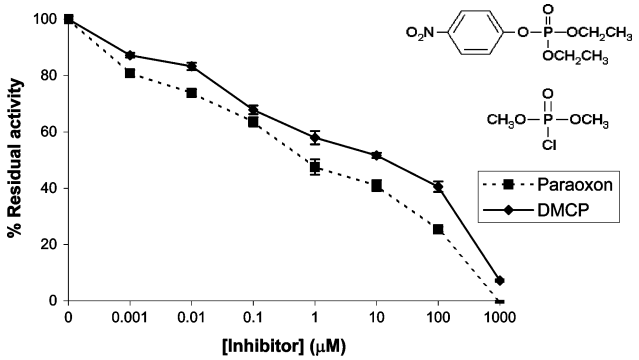

FIGURE 4: Inhibition of AeCXE1 by organophosphates. The percent residual activity of AeCXE1 toward 4MU butyrate (10 μM) is plotted as a function of paraoxon or dimethyl chlorophosphate (DMCP) concentration. Reactions were carried out in 25 mM Tris-Cl (pH 8.0) buffer at 25 °C. The amount of active catalytic centers added per inhibition reaction was 0.0021 pmol. Error bars represent a percentage of the standard error of the mean calculated from a minimum of three replicates over three experiments. Chemical structures are shown for paraoxon (above) and DMCP (below).

propriately in the oxyanion hole (Figure 5). Hydrogen bonds are observed between O1 and the main chain nitrogens of the oxyanion hole residues Gly92 (2.94 Å), Gly93 (2.75 Å), and Ala170 (2.85 Å). Of the two ethyl arms of the bound paraoxon molecule, one extends out toward the surface of the protein while the second points to the acyl chain binding pocket within the catalytic gorge. The two ethyl substituents are stabilized by packing against the side chains of Leu222, Ile230, Trp231, and Met278, and these interactions may

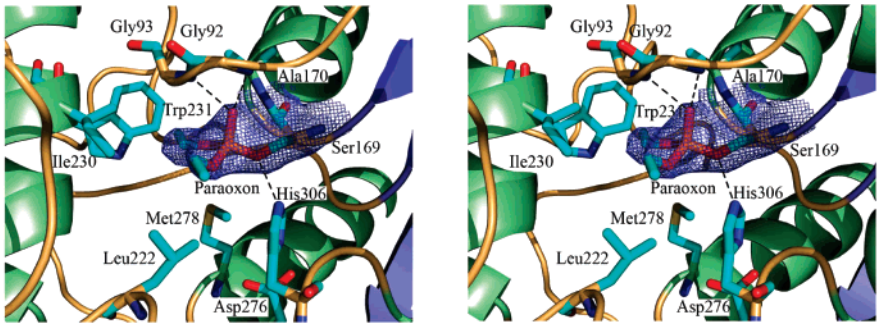

FIGURE 5: Stereoviews of the AeCXE1 catalytic gorge with the inhibitor paraoxon bound shown built into its electron density from a bias-removed $2F_o - F_c$ omit map, contoured at 1.5σ. Key residues of the catalytic gorge are shown as sticks with the hydrogen bonds shown as dashed black lines. This image was generated using Pymol (*48*).

explain the higher affinity of paraoxon, relative to that of the smaller DMCP.

The native and the paraoxon-bound structures of AeCXE1 superimpose closely at all Cα positions with a root-mean-square deviation (rmsd) of 0.27 Å. The only significant change between the two structures is a small upward shift (~1 Å) of His306 in the AeCXE1−paraoxon structure, allowing the carbonyl oxygen of the tetrahedral intermediate to form hydrogen bonds with the oxyanion hole residues and stabilizing the enzyme−inhibitor complex.

DISCUSSION

Bioinformatic analyses of the genome of the model plant *Ar. thaliana* (*12*) identified a total of 20 putative carboxylesterase genes. These were found to contain sequence motifs that pointed to the α/β-hydrolase fold, a characteristic structure that is shared by many proteases, lipases, esterases, and related enzymes (*17*). Phylogenetic analysis of these and other plant carboxylesterases showed that they could be grouped into seven clades (*12*), and subsequent searches of EST databases have shown that they form a large family that is found throughout the plant kingdom (data not shown). Functional investigations of members of this family have demonstrated roles in plant defense, plant development, and secondary metabolism (*14*−*16*, *35*−*39*). The carboxylesterase from *A. eriantha* (kiwifruit), the subject of this investigation, falls into clade II of the *Ar. thaliana* carboxylesterases (*12*). The only other carboxylesterase to have been studied from this clade, PepEST from *Capsicum annum*, has been shown to be upregulated in fungal infections (*14*).

The three-dimensional structure of AeCXE1 confirms it is a member of the α/β-hydrolase family. The structure reveals a typical Ser-His-Asp catalytic triad, comprising Ser169, His306, and Asp276, which are approached via a relatively deep active site gorge lined predominantly with hydrophobic residues. Our analysis also indicates that the AeCXE1 enzyme is most similar to the hormone-sensitive lipase (HSL) subfamily of α/β-hydrolases, which is named after a key mammalian metabolic enzyme (*40*). This family is characterized by a particular pattern of embellishments of the core α/β-hydrolase fold, notably an N-terminal extension and an inserted subdomain between strands β6 and β7 (*41*). The ESTHER database of α/β-hydrolase fold proteins [http://bioweb.ensam.inra.fr/esther/ (*42*)] shows that this family is currently mainly populated by bacterial and fungal representatives. To date, only one other plant esterase has also been characterized structurally, revealing it also to be a member of the α/β-hydrolase fold superfamily (*43*). This *S*-formylglutathione hydrolase is not a member of the CXE family but is distantly related; its sequence is 14% identical with that of AeCXE1 and contains one extra β-strand but fewer helices surrounding the central sheet. As more structures become available, it will be of interest to observe the prevalence of this fold, and the structural subfamilies that are found, among plant carboxylesterases and other enzymes.

Our functional assays confirm that AeCXE1 is indeed a carboxylesterase, with activity against a range of ester substrates, with acyl chain lengths ranging from 2 to 16 carbon atoms (acetate to palmitate). The presence of an adventitiously bound acyl intermediate in the native enzyme structure provides valuable clues to the structural basis of specificity. With the acyl oxygen occupying the characteristic α/β-hydrolase oxyanion hole, the three-carbon chain attached to this intermediate reaches well into a hydrophobic binding pocket at the bottom of the catalytic gorge, lined with the side chains of Phe94, Leu222, Leu227, Ile230, Trp231, and Met278. The kinetic results, which show the highest specificity constant for butyrate, indicate specificity for short to medium-length acyl groups.

A notable feature of the kinetic results, however, is that the enzyme also hydrolyzes esters with acyl chains as long as 16 carbons (palmitate), albeit with much lower efficiency. Modeling experiments show that for longer chains, an alternative binding mode is possible; if palmitate is bound to the catalytic serine, its acyl chain can project outward rather than fitting into the acyl binding pocket in the catalytic gorge, which is utilized by both the short chain intermediate and paraoxon (data not shown). This proposed alternative binding mode for longer chain substituents makes use of a hydrophobic patch near the opening of the catalytic gorge and may explain the low K_m estimates for long acyl chain substrates. This patch is contributed by residues 18−24 from the N-terminal extension, which is a characteristic feature of HSL family enzymes. Unlike other members of the HSL subfamily, however, AeCXE1 does not have a hydrophobic lid, the wide opening to its catalytic gorge (Figure 5) allowing it to accommodate a large range of esters.

Other activities have also been found for members of the CXE carboxylesterase family in plants. Akashi et al. (*15*) have shown that as well as carboxylesterase activity, the HID enzyme of legumes has dehydratase activity. This enzyme has a Thr in the active site replacing the typical Ser and falls into clade III of the Marshall et al. (*12*) classification

of the plant CXE carboxylesterases. Docking of 2-hydroxyisoflavanone, the substrate used by the HID enzymes, into the active site of AeCXE1, using GOLD (*44*), gives a consistent fit in which the pairwise rms difference in atomic position is only 0.45 Å for 10 independent models. In this model, the ring carbonyl oxygen is located in the oxyanion hole, the chromane ring extends toward the back of the gorge, and the hydroxybenzyl ring points out to the opening of the gorge. Importantly, the hydrogen on chiral C3, adjacent to the carbonyl, is equidistant (2.8 Å) between the two active site residues Ser169 and His306. This provides structural support for the proposed mechanism (*15*), which involves hydrogen abstraction by the active site Thr in the HID enzymes (equivalent to Ser169 in AeCXE1) followed by abstraction of the C2 hydroxyl by the protonated His, to complete the elimination of water from the substrate.

Particularly relevant to plant developmental biology is the fact that the recently identified soluble receptor for gibberellin from rice, GID1, falls into clade IV of the CXE phylogeny of Marshall et al. (*12*) with *Arabidopsis* containing three orthologs (*16*). Intriguingly, although the GID1 sequence contained serine and aspartate residues in positions analogous to the catalytic triad residues of homologous enzymes, the essential histidine was replaced with valine, implying that disruption of the catalytic triad has enabled the substrate binding cavity to be used in a different capacity. When gibberellic acid (GA_3), a gibberellin which is bound by GID1, is docked into AeCXE1, as a model for GID1, it is found to fit wholly within the active site gorge, making contacts with the walls of the cavity. The GA_3 molecule measures approximately 10 Å in length and extends to the bottom of the cavity, making contacts with residues Phe94, Phe97, Glu168, Ser169, Ala170, Leu222, Leu227, Ile230, Met278, His306, and Ala307.

Finally, early work on animal carboxylesterases led to a classification of these enzymes according to their interactions with organophosphates (*45*, *46*). In this classification scheme, carboxylesterases are grouped into class A esterases which hydrolyze organophosphates, class B esterases which are inhibited by organophosphates, class C esterases which do not interact with organophosphates, and class D esterases which also do not react with organophosphates but are sensitive to thiol alkylating reagents. For both class A and B carboxylesterases, the organophosphates act as substrates in that they can bind to their nucleophilic serine residues. However, while the A esterases have the ability to hydrolyze the organophosphates, the nucleophilic serine of the B esterases is phosphorylated by organophosphates, preventing the enzyme reaction from proceeding further. We have shown here that AeCXE1 is inhibited by the organophosphates paraoxon and dimethyl chlorophosphate (DMCP) and that paraoxon binds covalently to the active site serine, Ser169, through its phosphate group, in a binding that mimics the first tetrahedral intermediate of the carboxylesterase reaction mechanism. Paraoxon is used commercially as a crop protectant against insects, through application of its thiol form, parathion, which is converted to its active metabolite paraoxon. The field concentrations of parathion residues commonly found on apple leaves can be as high as 360 mM, some 10^3-10^4 times higher than the estimated IC_{50} for AeCXE1 (*47*). This suggests that commercial use of parathion and/or paraoxon could inhibit these carboxylesterases in plants, assuming residue concentrations inside the leaf are similar to those on its outside, with possible effects on plant growth and development. Interestingly, the *S*-formylglutathione hydrolase characterized by Cummins et al. (*43*) is insensitive to paraoxon but sensitive to thiol alkylating reagents due to the presence of a reactive Cys in the active site of the enzyme. This D esterase would therefore not be affected by exposure to organophosphate insecticides unlike the CXE carboxylesterases.

In conclusion, the structure of AeCXE1 has shown that the plant CXE carboxylesterases are members of the α/β-hydrolase superfamily of proteins and has demonstrated the structural basis of acyl specificity and the mode of inhibition by the insecticide paraoxon. Although further mutagenesis and biochemical studies are needed to better understand the substrate specificity and function of plant CXE carboxylesterases, this structural information can be used as a starting point to better understand these widely distributed enzymes and determine how they perform their various roles in plants.

ACKNOWLEDGMENT

We thank Dr. David Goldstone for synchrotron data collection at Stanford Synchrotron Radiation Laboratory. We gratefully acknowledge Michelle Williams and Drs. Irene Horne, Erica Crone, Dave Greenwood for discussions on esterase biochemistry, and Marcus Davy and Dr. Nihal DeSilva for assistance with statistical analysis.

REFERENCES

1. Taylor, P., and Radic, Z. (1994) The cholinesterases: From genes to proteins, *Annu. Rev. Pharmacol. Toxicol. 34*, 281−320.
2. Vogt, R. G., Riddiford, L. M., and Prestwich, G. D. (1985) Kinetic properties of a sex pheromone-degrading enzyme: The sensillar esterase of *Antheraea polyphemus*, *Proc. Natl. Acad. Sci. U.S.A. 82*, 8827−8831.
3. Hemingway, J. (2000) The molecular basis of two contrasting metabolic mechanisms of insecticide resistance, *Insect Biochem. Mol. Biol. 30*, 1009−1015.
4. Satoh, T., and Hosokawa, M. (1998) The mammalian carboxylesterases: From molecules to functions, *Annu. Rev. Pharmacol. Toxicol. 38*, 257−288.
5. Turner, J. M., Larsen, N. A., Basran, A., Barbas, C. F., III, Bruce, N. C., Wilson, I. A., and Lerner, R. A. (2002) Biochemical characterization and structural analysis of a highly proficient cocaine esterase, *Biochemistry 41*, 12297−12307.
6. Sussman, J. L., Harel, M., Frolow, F., Oefner, C., Goldman, A., Toker, L., and Silman, I. (1991) Atomic structure of acetylcholinesterase from *Torpedo californica*: A prototypic acetylcholine-binding protein, *Science 253*, 872−879.
7. Redinbo, M. R., and Potter, P. M. (2005) Mammalian carboxylesterases: From drug targets to protein therapeutics, *Drug Discovery Today 10*, 313−325.
8. Tanksley, S. D., and Rick, C. M. (1980) Genetics of esterases in species of *Lycopersicon*, *Theor. Appl. Genet. 56*, 209−219.
9. Manganaris, A. G., and Alston, F. H. (1992) Genetics of esterase isoenzymes in *Malus*, *Theor. Appl. Genet. 83*, 467−475.
10. Fachinello, J. C., Musacchi, S., Zuccherelli, S., and Sansavini, S. (2000) Isoenzymatic variability in pear tissues for fingerprinting, *Pesqui. Agropecu. Bras. 35*, 1427−1432.
11. Akoh, C. C., Lee, G. C., Liaw, Y. C., Huang, T. H., and Shaw, J. F. (2004) GDSL family of serine esterases/lipases, *Prog. Lipid Res. 43*, 534−552.
12. Marshall, S. D. G., Putterill, J. J., Plummer, K. M., and Newcomb, R. D. (2003) The carboxylesterase gene family from *Arabidopsis thaliana*, *J. Mol. Evol. 57*, 487−500.
13. Forouhar, F., Yang, Y., Kumar, D., Chen, Y., Fridman, E., Park, S. W., Chiang, Y., Acton, T. B., Montelione, G. T., Pichersky, E., Klessig, D. F., and Tong, L. (2005) Structural and biochemical studies identify tobacco SABP2 as a methyl salicylate esterase

and implicate it in plant innate immunity, *Proc. Natl. Acad. Sci. U.S.A. 102*, 1773−1778.
14. Kim, Y. S., Lee, H. H., Ko, M. K., Song, C. E., Bae, C. Y., Lee, Y. H., and Oh, B. J. (2001) Inhibition of fungal appressorium formation by pepper (*Capsicum annuum*) esterase, *Mol. Plant−Microbe Interact. 14*, 80−85.
15. Akashi, T., Aoki, T., and Ayabe, S. (2005) Molecular and biochemical characterization of 2-hydroxyisoflavanone dehydratase. Involvement of carboxylesterase-like proteins in leguminous isoflavone biosynthesis, *Plant Physiol. 137*, 882−891.
16. Ueguchi-Tanaka, M., Ashikari, M., Nakajima, M., Itoh, H., Katoh, E., Kobayashi, M., Chow, T. Y., Hsing, Y. I., Kitano, H., Yamaguchi, I., and Matsuoka, M. (2005) GIBBERELLIN INSENSITIVE DWARF1 encodes a soluble receptor for gibberellin, *Nature 437*, 693−698.
17. Ollis, D. L., Cheah, E., Cygler, M., Dijkstra, B., Frolow, F., Franken, S. M., Harel, M., Remington, S. J., Silman, I., Schrag, J., Sussman, J. L., Verschueren, K. H. G., and Goldman, A. (1992) The α/β hydrolase fold, *Protein Eng. 5*, 197−211.
18. Heikinheimo, P., Goldman, A., Jeffries, C., and Ollis, D. L. (1999) Of barn owls and bankers: A lush variety of α/β hydrolases, *Strucuture 7*, R141−R146.
19. Nardini, M., and Dijkstra, B. W. (1999) α/β hydrolase fold enzymes: The family keeps growing, *Curr. Opin. Struct. Biol. 9*, 732−737.
20. Holmquist, M. (2000) α/β-Hydrolase fold enzymes: Structures, functions and mechanisms, *Curr. Protein Pept. Sci. 1*, 209−235.
21. Moreland, N., Ashton, R., Baker, H. M., Ivanovic, I., Patterson, S., Arcus, V. L., Baker, E. N., and Lott, J. S. (2005) A flexible and economical medium-throughput strategy for protein production and crystallization, *Acta Crystallogr. D61*, 1378−1385.
22. Otwinowski, Z., and Minor, W. (1997) Processing of X-ray diffraction data collected in oscillation mode, *Methods Enzymol. 276*, 307−326.
23. Leslie, A. G. W. (1992) Recent changes to the MOSFLM package for processing film and image plate data, *Newsletter on Protein Crystallography*, Vol. 26, Science and Engineering Research Council, Daresbury Laboratory, Warrington, U.K.
24. Terwilliger, T. C., and Berendzen, J. (1999) Automated MAD and MIR structure solution, *Acta Crystallogr. D55*, 849−861.
25. Terwilliger, T. C. (1999) Reciprocal-space solvent flattening, *Acta Crystallogr. D55*, 1863−1871.
26. Terwilliger, T. C. (2000) Maximum likelihood density modification, *Acta Crystallogr. D56*, 965−972.
27. Lamzin, V. S., and Wilson, K. S. (1997) Automated refinement for protein crystallography, *Methods Enzymol. 277*, 269−305.
28. Emsley, P., and Cowtan, K. (2004) Coot: Model-Building Tools for Molecular Graphics, *Acta Crystallogr. D60*, 2126−2132.
29. Murshudov, G. N., Vagin, A. A., and Dodson, E. J. (1997) Refinement of macromolecular structures by the maximum-likelihood method, *Acta Crystallogr. D53*, 240−255.
30. Laskowski, R. A., MacArthur, M. W., Moss, D. S., and Thornton, J. M. (1993) PROCHECK: A program to check the stereochemical quality of protein structures, *J. Appl. Crystallogr. 26*, 283−291.
31. Krissinel, E., and Henrick, K. (2004) Secondary-structure matching (SSM), a new tool for fast protein structure alignment in three dimensions, *Acta Crystallogr. D60*, 2256−2268.
32. De Simone, G., Menchise, V., Manco, G., Mandrich, L., Sorrentino, N., Lang, D., Rossi, M., and Pedone, C. (2001) The crystal structure of a hyper-thermophilic carboxylesterase from the archaeon *Archaeoglobus fulgidus*, *J. Mol. Biol. 314*, 507−518.
33. De Simone, G., Galdiero, S., Manco, G., Lang, D., Rossi, M., and Pedone, C. (2000) A snapshot of a transition state analogue of a novel thermophilic esterase belonging to the subfamily of mammalian hormone-sensitive lipase, *J. Mol. Biol. 303*, 761−771.
34. Wei, Y., Contreras, J. A., Sheffield, P., Østerlund, T., Derewenda, U., Kneusel, R. E., Matern, U., Holm, C., and Derewenda, Z. S. (1999) Crystal structure of Brefeldin A esterase, a bacterial homolog of the mammalian hormone-sensitive lipase, *Nat. Struct. Biol. 6*, 340−345.
35. Pontier, D., Godiard, L., Marco, Y., and Roby, D. (1994) *hsr203J*, a tobacco gene whose activation is rapid, highly localized and specific for incompatible plant/pathogen interactions, *Plant J. 5*, 507−521.
36. Pontier, D., Tronchet, M., Rogowsky, P., Lam, E., and Roby, D. (1998) Activation of hsr203, a plant gene expressed during incompatible plant-pathogen interactions, is correlated with programmed cell death, *Mol. Plant−Microbe Interact. 11*, 544−554.
37. Walden, A. R., Walter, C., and Gardner, R. C. (1999) Genes expressed in *Pinus radiata* male cones include homologs to anther-specific and pathogenesis response genes, *Plant Physiol. 121*, 1103−1116.
38. Ichinose, Y., Hisayasu, Y., Sanematsu, S., Ishiga, Y., Seki, H., Toyoda, K., Shiraishi, T., and Yamada, T. (2001) Molecular cloning and functional analysis of pea cDNA *E86* encoding homologous protein to hypersensitivity-related *hsr203J*, *Plant Sci. 160*, 997−1006.
39. Bezier, A., Lambert, B., and Baillieul, F. (2002) Cloning of a grapevine Botrytis-responsive gene that has homology to the tobacco hypersensitivity-related *Hsr203J*, *J. Exp. Bot. 53*, 2279−2280.
40. Vaughn, M., Berger, J. E., and Steinberg, D. (1964) Hormone-sensitive lipase and monoglyceride lipase activities in adipose tissue, *J. Biol. Chem. 239*, 401−409.
41. Osterlund, L. T., Danielsson, B., Degerman, E., Contreras, J. A., Edgren, G., Davis, R. C., Schotz, M. C., and Holm, C. (1996) Domain-structure analysis of recombinant rat hormone-sensitive lipase, *Biochem. J. 319*, 411−420.
42. Hotelier, T., Ludovic, R., Xavier, C., Vincent, N., Pascale, M., and Chatonnet, A. (2004) ESTHER, the database of the α/β-hydrolase fold superfamily of proteins, *Nucleic Acids Res. 32*, D145−D147.
43. Cummins, I., McAuley, K., Fordham-Skelton, A., Schwoerer, R., Steel, P. G., Davis, B. G., and Edwards, R. (2006) Unique Regulation of the Active site of the Serine Esterase S-Formylglutathione Hydrolase, *J. Mol. Biol. 359*, 422−432.
44. Verdonk, M. L., Cole, J. C., Hartshorn, M. J., Murray, C. W., and Taylor, R. D. (2003) Improved protein-ligand docking using GOLD, *Proteins: Struct., Funct., Genet. 52*, 609−623.
45. Aldrige, W. N. (1953) Serum esterases. I. Two types of esterase (A and B) hydrolysing p-nitrophenyl acetate, propionate and butyrate, and a method for their determination, *Biochem. J. 53*, 110−117.
46. Walker, C. H. (1989) The development of an improved system of nomenclature and classification of esterases, in *Enzymes Hydrolyzing Organophosphorous Compounds* (Reiner, E., Aldrige, W. N., and Hoskin, F. C. G., Eds.) pp 236−245, Ellis Horwood Ltd., New York.
47. Hoerger, F. D., and Kenaga, E. E. (1972) Pesticide residues on crops: Correlation of representative data as a basis of their estimation of their magnitude in the environment, in *Environmental Quality and Safety: Chemistry, Toxicology, and Technology* (Coulston, F., and Korte, F., Eds.) pp 9−28, Academic Press, New York.
48. DeLano, W. L. (2002) *The PyMOL Molecular Graphics System*, DeLano Scientific, San Carlos, CA.
49. Devonshire, A. L., Heidari, R., Bell, K. L., Campbell, P. M., Campbell, B. E., Odgers, W. A., Oakeshott, J. G., and Russell, R. J. (2003) Kinetic efficiency of mutant carboxylesterases implicated in organophosphate insecticide resistance, *Pest. Biochem. Physiol. 76*, 1−13.

BI062046W